PROFESSOR STANISLAV GOBEC (Orcid ID : 0000-0002-9678-3083)

Article type : Research Article

In silico identification, synthesis and biological evaluation of novel tetrazole inhibitors of MurB

Martina Hrast[a], Marko Jukič[a], Delphine Patin[b], Julie Tod[c], Christopher G Dowson[c], David I Roper[c], Hélène Barreteau[b] and Stanislav Gobec[a]

Corresponding author: Stanislav Gobec; phone: +386 1 476 9585; fax: +386 1 425 8031; e-mail: Stanislav.gobec@ffa.uni-lj.si

[a] Department of Medicinal Chemistry; Faculty of Pharmacy, University of Ljubljana, Aškerčeva 7, SI-1000, Ljubljana, Slovenia

[b] Group Bacterial Cell Envelopes and Antibiotics; Institute for Integrative Biology of the Cell (I2BC), CEA, CNRS, Univ Paris Sud, Université Paris-Saclay, 91198 Gif-sur-Yvette cedex, France

[c] School of Life Sciences; University of Warwick, Coventry, CV4 7AL, UK

Keywords: in-silico, virtual screening, pharmacophore modeling, antibacterial agents, peptidoglycan, MurB

Abstract: In the context of antibacterial drug discovery resurgence, novel therapeutic targets and new compounds with alternative mechanisms of action are of paramount importance. We focused on UDP-*N*-acetylenolpyruvylglucosamine reductase (i.e. MurB), an underexploited target enzyme that is involved in early steps of bacterial peptidoglycan biosynthesis. On the basis of the recently reported crystal structure of MurB in complex with $NADP^+$, a pharmacopohore model was generated and used in a virtual screening campaign with combined structure-based and ligand-based approaches. In order to explore chemical space around hit compounds, further similarity search and organic synthesis was employed to obtain several compounds with micromolar IC_{50} values on MurB. The best inhibitors in the reported series of 5-substituted tetrazol-2-yl acetamides were compounds **13**, **26** and **30** with IC_{50} values of 34, 28 and 25 μM, respectively. None of the reported compounds possessed *in vitro* antimicrobial activity against *S. aureus* and *E. coli*.

This article has been accepted for publication and undergone full peer review but has not been through the copyediting, typesetting, pagination and proofreading process, which may lead to differences between this version and the Version of Record. Please cite this article as doi: 10.1111/cbdd.13172

Introduction

Recently, resurgence in antibacterial drug discovery can be observed, especially in the context of emerging resistant bacteria.[1] Resistant and multi-drug resistant pathogens are reported globally in general community and hospitals, which makes novel antibacterial discovery an immediate and important endeavour.[2] A steady stream of innovative molecular scaffolds, revisits of the older data, unification of interdisciplinary drug-discovery approaches and utilisation of underexploited therapeutic targets are decisive approaches in our pursuit of novel drugs.[3-5] Among the most important and underutilised therapeutic targets in antibacterial drug discovery are early steps of bacterial cell wall biosynthesis.[6]

Peptidoglycan is a key component of bacterial cell wall. It provides bacteria with the necessary structural integrity to withstand the osmotic pressure gradient between the cytoplasm and the cell exterior. It is composed of alternating disaccharide units of *N*-acetyl muramic acid (Mur*N*Ac) and *N*-acetyl glucosamine (Glc*N*Ac) that are cross-linked with short peptide chains.[7] Peptidoglycan biosynthesis requires approximately 20 reactions, catalysed by different enzymes.[8] Each enzyme in this pathway is essential and unique for bacteria and thus important and selective target for the discovery of new antibacterial agents.[9,10]

In this work, we have focused on the UDP-*N*-acetylenolpyruvylglucosamine reductase or MurB.[11] The enzyme reduces the enolpyruvyl moiety of UDP-*N*-acetyl glucosamine-enolpyruvate (UDP-Glc*N*Ac-EP), produced by MurA (Figure 1). MurB contains one molecule of non-covalently bound flavin adenine dinucleotide (FAD) that, during the catalytic process, serves as a hydride transfer mediator between *β*-nicotinamide dinucleotide phosphate (NADPH) and the enolpyruvyl substrate. First, NADPH binds to the enzyme and transfers the 4-*pro*-S hydrogen to *N*-5 atom of the enzyme-bound FAD, then $NADP^+$ dissociates from the enzyme. In the second half-reaction, substrate UDP-Glc*N*Ac-EP binds to MurB with the following hydride transfer from $FADH_2$ to vinyl ether of the UDP substrate, forming UDP-*N*-acetyl muramic acid (UDP-Mur*N*Ac).[12]

Figure 1: Catalytic consecutive and two-step mechanism of MurB.

There are only few MurB inhibitors present in the literature and compounds **1** and **2** (Figure 2) were among the first reported. Imidazolinone **2** is a result of optimisation campaign where the heterocycle core replaced the starting 4-thiazolidinone moiety. Both heterocycles were designed to mimic the diphosphate moiety of UDP-Glc*N*Ac-EP substrate.[13, 14] Compound **3** (Figure 2) was identified by high-throughput (HTS) screening as MurB inhibitor with low micromolar K_d value. [15] Furthermore, alkyl pyrazolidinedione derivatives were found as good inhibitors of *S. aureus* and *E. coli* MurB (e.g. **4**, Figure 2).[16, 17] A series of phenyl thiazolyl urea (e.g. **5**, Figure 2) and carbamate analogues inhibited the enzyme in the low micromolar range.[18] Most published MurB inhibitors possessed promising antibacterial activities, however, when tested in the presence of 4% bovine serum albumin, their activities were lost, indicating high-protein binding properties of compounds. No novel inhibitors of MurB have been reported in the last decade, while the compounds described above were not pursued further due to their unfavourable physico-chemical properties. Therefore we sought to identify novel compounds with improved physico-chemical properties and greater optimisation potential. Overall, MurB is an

attractive target in antibacterial drug discovery and herein we here report a successful pharmacophore-based *in-silico* study that led to the discovery of novel structural class of MurB inhibitors.

Figure 2: Previously described MurB inhibitors present in the scientific literature.

Methods and Materials

Pharmacophore preparation and Virtual Screening: Protocol consisted of pharmacophore modelling, compound collection from ZINC version 12, database preparation and virtual screening.[19] Pharmacophore models can be described as representation or 3D-arrangement of the chemical features and steric limitations, postulated as necessary for a small molecule to interact with its target.[20] These features are presented in Figure 3 and Figure 4. MurB with non-covalently bound FAD and active site defined as space occupied by NADP (PDB IDs: 4JAY, 4JB1) was used in an automatic generation of three-dimensional structure-based pharmacophore using an effective LigandScout (Software-Entwicklungs und Consulting GmbH, Maria Enzersdorf, Austria) software package. Ten or less pharmacophoric features were used for pharmacophore generation with additional generation of exclusion volume spheres on the basis of available space at the active site. Resulting models are depicted in Figure 3.[21]

Figure 3: Left: pharmacophore, created on the basis of NADP, chain A (PDB ID: 4JAY) with superposed shared pharmacophore with UDP-Glc*N*Ac-EP (PDB ID: 2MBR). Middle: pharmacophore, created with superposed NADP. Right: pharmacophore, created with added exclusion sphere coat representing the available space in the active site (yellow – planar/aromatic with tolerance sphere of 1.5 Å, red – H-bond acceptor with vector and tolerance sphere of 1.5 Å, green – H-bond donor with vector and tolerance sphere of 1.5 Å, centered red sphere – ionisable feature with tolerance of 2.15 Å, grey – exclusion spheres with tolerance of 1 Å).

The created pharmacophore was validated with the superposition and analysis of MurB in complex with UDP-Glc*N*Ac-EP.[22] Upon structural analysis, NADP (PDB ID: 4JB1; Figure 4) presents the nicotinamide terminal moiety in the close proximity to the FAD flavin mononuleotide *N*-5 atom and Glu335 and Ser239 residues, consecutively enabling the transfer of hydride for the reduction of FAD. Similar positioning can be observed for the substrate UDP-Glc*N*Ac-EP (PDB ID: 2MBR) where the terminal carboxyvinyl moiety occupies the same space and the alkene fragment is positioned in close proximity to the *N*-5 atom of FAD(H_2) and Glu325 and Ser229 residues, for final substrate reduction towards UDP-Mur*N*Ac and NADP. Other terminus of both substrates diverged positionally and uridine diphosphate or adenine diphosphate nucleotides were observed at distinct binding modes for UDP-Glc*N*Ac-EP and NADP, respectively. Using LigandScout software, a three dimensional pharmacophore for UDP-Glc*N*Ac-EP in the active site was created, aligned to preceding pharmacophore model based on nicotinamide dinucleotide phosphate and a shared pharmacophore created, i.e. pharmacophore where individual pharmacophoric elements are shared by multiple structures. The produced final shared 3D pharmacophore model was superimposed on the starting pharmacophore model and was found to be nearly identical apart from terminal H-bond donor/acceptor motif typical of terminal carboxamide (Figure 1, left).[23] The final production pharmacophore model based on the MurB in complex with $NADP^+$ (PDB ID

4JAY) was thus refined by removing features, adjusting the tolerance sphere size and definition of exclusion spheres around the nicotinamide adenine dinucleotide phosphate (Figure 4).

Figure 4: Left: superposition of UDP-Glc*N*Ac-EP (blue, PDB ID: 2MBR) and NADP (cyan with coloured atom types, PDB ID: 4JAY); FAD can be observed in almost identical binding mode. Right: calculated pharmacophore: hydrophobic 46.571907, -5.837457, 11.458156; ionisable 45.4222 -11.2288 11.2484; ionisable 45.8758 -13.7696 11.946; HBA 52.896 -10.663 12.334, 50.177 -10.402 13.677; HBA 53.257 -9.782 15.791, 50.177 -10.402 13.677; HBA 47.614 -13.199 7.989, 47.208 -13.871 11.119; HBA 43.817, -13.738, 7.969, 45.229 -11.925 9.78; HBA 47.614 -13.199 7.989, 45.229 -11.925 9.78; HBA 43.132 -3.175 13.229, 45.933 -2.903 13.325; HBD 47.234 -3.916 14.773; 46.564 -1.598 16.459.

Compounds were collected from ZINC 12 as Drugs Now subset (11 538 905 compounds) and database for the virtual screening protocol was prepared with consecutive filtering steps. First, the database was checked for PAINS (pan-assay interference compounds) and known and predicted aggregators were filtered out using FILTER software from OpenEye (OpenEye Scientific Software, Inc., Santa Fe, NM, USA; www.eyesopen.com). [24,25] Database was further pruned to eliminate structural faults, metals (metal complexes) and reactive functional groups that would pose frequent-hitter and high reactivity problems.[26] Molecules with molecular mass between 250-800 Da were retained to obtain a final collection of 4 755 936 compounds. Three-dimensional conformer database was prepared with OpenEye (OpenEye Scientific Software, Inc., Santa Fe, NM, USA; www.eyesopen.com) OMEGA2 omega-fast protocol. Maximum number of conformations was set at 25, rms threshold of 0.8 was used and energy window of 10 with 4000 max pool size with ring and nitrogen enumeration, molecules were used as reported in ZINC database without calculating all possible tautomer structures and ionizations.[27] Final LigandScout ldb database was created using Idbgen software from Inte:Ligand (Software-Entwicklungs und Consulting GmbH, Maria Enzersdorf, Austria) (Figure 5).

Figure 5: Preparation of ZINC database for virtual screening step using LigandScout.

Virtual screening was performed using Inte:Ligand LigandScout software with Pharmacophore-Fit scoring function. Exclusion spheres were considered in the calculation with minimum of three required pharmacophoric features. Top ranked and commercially available compounds were purchased (Table 1) and biologically evaluated as described below. Amongst 12 purchased and biologically evaluated compounds a hit compound **13** was identified, and IC_{50} value was determined to be 34 µM on MurB.

Molecular docking: Compounds were evaluated by FILTER 2.5.1.4 software (OpenEye Scientific Software, Inc., Santa Fe, NM, USA; www.eyesopen.com) for possible aggregation properties. 3D conformer library was generated with OMEGA2 2.5.1.4 software from OpenEye with 3000 maximum conformations per compound, rms of 0.5 and considered all possible stereoisomers of compounds.[27] Receptor was prepared from X-ray crystal structure of MurB in complex with $NADP^+$ (PDB ID: 4JAY) active site, chain A with Make Receptor 3.2.0.2 software from OpenEye (OpenEye Scientific Software, Inc., Santa Fe, NM, USA; www.eyesopen.com)

with FAD molecule in-place. Box with the volume of 7791 $Å^3$ (17.00 × 25.00 × 18.33 Å) around $NADP^+$ ligand was defined and balanced shape potential calculated. Pocket volume was 1403 $Å^3$ and no constraints were used in docking runs. First, NAP co-crystalized substrate was extracted from the receptor and re-docking experiment was performed for validation of experiment. 3D conformer library for the NAP substrate (PDB ID: 4JAY) was prepared using Omega2 from OpenEye (3000 conformations, RMS 0.5, flipper true parameters) and the substrate was re-docked with HYBRID 3.2.0.2 from OpenEye OEDocking module with high resolution docking parameter enabled. Reproduction of experimentally determined binding mode (PDB ID: 4JAY) with an RMSD of 0.605 Å was successful. Then, an enrichment study was performed using a 3D conformer library of reported tetrazoles and a libraray of 1000 decoy molecules prepared by Schrödinger (Omega2 from OpenEye, validation experiment parameters).[28] Both libraries were docked for further binding mode studies and all active compounds (**25**, **18**, **22**, **30**, **26** and **13**) were ranked at the top 6 % of the entire decoy-test library.

Analogue identification: With the OpenBabel software, a path-based fingerprint FP2 which indexes linear fragments of up to 7 atoms (similar to the Daylight fingerprints) was calculated for the main ZINC compound vendor catalogues (namely Enamine, ChemBridge, Vitas-M and Princeton Biomolecular Research) and fast search index created for the compound databases . Finally the created databases were searched for compounds with similar chemical space to the query compound **13**.[29]

Cloning, overproduction and purification of MurB from *E. coli*: The *E. coli murB* gene was amplified from a DH5α strain (Invitrogen) using the primers 5'- GCGT**GAATTC**ATGAACCACTCCTTAAAACCC-3' and 5'-CTAC**AAGCTT**TCATGAAATTGTCTCCACTGCGC -3'. The primer upstream of the start codon (underlined) contained an engineered EcoRI site (in bold). The primer 3' to the gene contained an engineered HindIII site (in bold). The amplified product was digested by EcoRI and HindIII and inserted between the compatible EcoRI and HindIII sites in vector pET2130 (T7 promoter), generating a plasmid that encodes MurB with a His_6 N-terminal extension. The construction was verified by DNA sequencing (Eurofins-MWG). Plasmid pET2130::$murB_{Ec}$ was transformed into *E. coli* BL21(DE3) (Novagen) for expression experiments.[30]

An overnight preculture of *E. coli* BL21(DE3) harbouring pET2130::*murB* was used to inoculate 1 liter of 2YT supplemented with 100 µg mL^{-1} ampicillin. The culture was incubated at 37°C with shaking until the optical density at 600 nm reached 0.8. Isopropyl ß-D-thiogalactopyranoside was added at a final concentration of 1 mM, and incubation was continued for 3 h at 37°C with shaking. The cells were harvested at 4°C, and the pellet was washed with cold 20 mM phosphate buffer, pH 7.2, containing 1 mM dithiothreitol (buffer A). Bacteria were resuspended in buffer A (10 mL) and disrupted by sonication in the cold. The resulting suspension was centrifuged at 4°C for 30 min at 200,000 *g* and the pellet was discarded. The supernatant was kept at -20°C.
The His_6-tagged MurB protein was purified on Ni^{2+}-nitrilotriacetate-agarose following the manufacturer's recommendations (Qiagen). All procedures were performed at 4°C. The supernatant was mixed for 1 h with the polymer, which had previously been washed with buffer A containing 0.3 M KCl and 10 mM imidazole. The washing and elution steps were performed with a discontinuous gradient of imidazole (20-300 mM) in buffer A containing 0.3 M KCl. Protein contents were analyzed by sodium dodecyl sulfate-polyacrylamide gel

electrophoresis. Relevant fractions were pooled and dialyzed against buffer A. Glycerol (10% final concentration) was added for storage of the protein at -20°C.

MurB inhibition assay: The inhibition of MurB enzyme was measured with a continuous assay by monitoring the oxidation of NADPH.[30] The reaction mixture with final volume of 200 µL contained 50 mM Tris-HCl (pH 8.0), 10 mM KCl, 100 µM NADPH, 50 µM UDP-Glc*N*Ac-EP, and 100 µM of compound dissolved in DMSO. All of the compounds were soluble in the final assay mixture containing 2% of DMSO (v/v). The reaction was initiated by the addition of enzyme. The decrease in absorbance at 340 nm was monitored over 10 min at 37 °C. The residual activity was calculated with respect to a similar assay without the inhibitors. All the experiments were performed in triplicates. The IC_{50} values were determined at seven different concentrations of inhibitor and were calculated from the fitted regression equations using the logit-log plot.

For the most active compound **30**, Ki determinations were performed under similar assay conditions as described above. First, the concentrations of NADPH (25, 50, 75, 100 and 200 µM) were varied at fixed concentration of UDP-Glc*N*Ac-EP (50 µM). Then the concentrations of UDP-Glc*N*Ac-EP (25, 50, 75 and 100 µM) were varied at fixed concentration of NADPH (100 µM). The concentrations of compounds **30** were 0, 10, 20, 30, 50, 75 and 100 µM. All experiments were performed in triplicates. The resulting data was analysed using the SigmaPlot 12 software and fitted to competitive, uncompetitive, non-competitive and mixed type inhibition models. The mode of inhibition and Ki values were chosen from the best ranking model, as calculated by the software. A representative graph depicting the best fit model for compound **30** is shown in Figure 6.

Figure 6: Lineweaver-Burk diagram of non-competitive binding mode of compound **30** versus NADPH. The concentrations of NADPH (25, 50, 75, 100 and 200 µM) were varied at fixed concentration of UDP-Glc*N*Ac-EP (50 µM). The concentrations of inhibitor were 0, 10, 20, 30, 50, 75 and 100 µM.

Microbiological evaluation: The antimicrobial activities for compounds were determined by broth microdilution in Luria Broth Miller (LB) against *S. aureus* (ATCC 29213) and *E. coli* (ATCC 25922). All of the experminents were performed according to CLSI guidelines and European Committee for Antimicrobial Susceptibility Testing recommendations.[31] Bacterial suspension of specific bacterial strain equivalent to 0.5 MacFarland turbidity standard (approximately 1×10^8 CFU/mL) was diluted with LB broth to obtain a final inocolum of 5×10^5 CFU/mL in the assay. The compounds were dissolved in DMSO and then diluted 40-fold in LB, just before use. Bacterial suspension and test compound solution were mixed together in the 96-well plate (final volume, 200 µL) and incubated for 18-24 h at 37 °C. Optical density was measured at 600 nm and was used for evaluating the antimicrobial activity of tested compounds by comparing to untreated control. The MIC values were determined as the lowest dilutions of the compounds showing no turbidity.

Reagents and analytics: All of the chemicals used were obtained from commercial sources (Acros, Aldrich, Alfa Aeser, Fluka), and were used without further purification. Solvents were used without purification or drying, unless otherwise stated. Reactions were monitored using analytical thin-layer chromatography plates (Merck, silica gel 60 F254, 0.25 mm), and the compounds were visualized with ultraviolet light and ninhydrin staining reagent. Silica gel grade 60 (particle size 0.040-0.063 mm; Merck, Germany) was used for flash-column chromatography. ^{1}H and ^{13}C NMR spectra were recorded on a Bruker AVANCE III 400 MHz spectrometer in

$CDCl_3$ and DMSO-d_6, solvents respectively, with TMS as the internal standard. Mass spectra were obtained with a VG-Analytical Autospec Q mass spectrometer (Centre for Mass Spectrometry, Institute Jožef Stefan, Ljubljana). Melting points were determined using a Reichert hot-stage microscope, and are uncorrected. HPLC analyses were performed on a Thermo Scientific Dionex UltiMate 3000 system (Thermo Fisher Scientific Inc., Waltham, MA, USA), using an Agilent Eclipse Plus C18 column (5 µm, 4.6 × 150 mm), at a flow rate of 1.5 mL/min, temperature 25 °C and injection volume of 10 µL. The eluent was a mixture of 0.1% TFA in water (A) and acetonitrile (B). The gradient was 10% B to 90% B in 15 min, then 90% B for 5 min. The purity of the tested compounds was established to be ≥95%.

Chemistry: Hit compound **13** (Table 2) was resynthesized along with four additional compounds (**18**, **24**, **25** and **30**; Table 2). Key 5-(4-chlorophenyl)-*1H*-tetrazole intermediate **13a** (Figure 7) was prepared by treatment of nitrile with sodium azide and ammonium chloride. *N*-Chloroacetamides were synthesized from different anilines and chloroacetyl chloride. All 2,5-disubstituted tetrazoles were obtained from *N*-chloroacetamides and tetrazole in ethanol in the presence of KOH. Finally, nitriles were converted to amides using alkaline hydrogen peroxide (Figure 7).[32]

Figure 7: Synthesis of tetrazoles. Reagents and conditions: (a) NaN_3, NH_4Cl, DMF, 120 °C, 18 h; (b) chloroacetyl chloride, TEA, DCM, 0°C - rt, 6 h; (c) KOH, EtOH, reflux, 16 h; (d) 30% H_2O_2, 1 M NaOH, DMSO, 0 °C - rt, 4 h.

5-(4-Chlorophenyl)-1H-tetrazole (**13a**): To a solution of 4-chlorobenzonitrile (3.0 g, 21.8 mmol) in DMF (15 mL), NaN_3 (1.56 g, 24.0 mmol) and NH_4Cl (1.28 g, 24 mmol) were added. The reaction mixture was stirred at 120 °C for 16 h. The mixture was cooled to room temperature, and 1 M HCl (50 mL) was added. The formed white solid was filtered off, washed with water, and dried at 60 °C for 18 h. Yield = 94%; ^{1}H NMR (400 MHz, DMSO-d_6): δ 8.60 (d, 2H, J = 8.6 Hz, 2 × Ar-H), 8.08 (d, 2H, J = 8.6 Hz, 2 × Ar-H) ppm.

General procedure for synthesis of compounds **24a**, **25a** and **30a**: To a solution of different anilines (8.5 mmol) in DCM (25 mL), TEA (2.35 mL, 16.9 mmol) was added and the mixture was cooled to 0°C. Chloroacetyl chloride (0.750 mL, 9.35 mmol) diluted in DCM (10 mL) was added dropwise and the mixture was stirred for 6 h at room temperature. To the reaction mixture, DCM (50 mL) was added and it was washed with water (50 mL), 1 M HCl (2 × 50 mL), saturated aqueous $NaHCO_3$ (50 mL) and brine (50 mL), dried with Na_2SO_4, and evaporated under reduced pressure. The solid was used without further purification.

2-Chloro-N-(3-cyanophenyl)acetamide (**24a**)*:* Yield = 61%; ^{1}H NMR (400 MHz, $CDCl_3$): δ 4.22 (s, 2H, CH_2), 7.46-7.50 (m, 2H, 2 × Ar-H), 7.73-7.76 (m, 1H, Ar-H), 8.00-8.01 (m, 1H, Ar-H), 8.34 (bs, 1H, NH) ppm.

2-Chloro-N-(4-cyanophenyl)acetamide (**25a**): Yield = 66%; ^{1}H NMR (400 MHz, DMSO-d_6): δ 4.32 (s, 2H, CH_2), 7.76-7.83 (m, 4H, 4 × Ar-H), 10.74 (bs, 1H, NH) ppm.

2-Chloro-N-phenylacetamide (**30a**): Yield = 73%; mp = 138-141°C (lit. 136-139 °C [32]); ^{1}H NMR (400 MHz, DMSO-d_6): δ 4.25 (s, 2H, CH_2), 7.09 (t, 1H, *J* = 7.4 Hz, Ar-H), 7.33 (t, 1H, *J* = 7.9 Hz, Ar-H), 7.59 (d, 2H, *J* = 7.8 Hz, 2 × Ar-H), 10.30 (bs, 1H, NH) ppm.

General procedure for synthesis of compounds **24**, **25** and **30**: To a solution of KOH (3.75 mmol) in ethanol (20 mL), 5-(4-chlorophenyl)-1*H*-tetrazole (2.5 mmol) and chloroacetamides (**24a**, **25a** or **30a**, 2.5 mmol) were added and the mixture was heated under reflux for 16 h. The reaction was cooled to room temperature and water (50 mL) was added. The formed precipitate was filtered off and recrystallized from ethanol to obtain pure final compounds.

2-(5-(4-Chlorophenyl)-2H-tetrazol-2-yl)-N-(3-cyanophenyl)acetamide (**24**): Yield = 51%; white solid, mp = 209-211°C; ^{1}H NMR (400 MHz, DMSO-d_6): δ 5.84 (s, 2H, CH_2), 7.58-7.61 (m, 2H, 2 × Ar-H), 7.66 (d, 2H, *J* = 8.6 Hz, 2 × Ar-H), 7.81-7.84 (m, 1H, Ar-H), 8.05-8.06 (m, 1H; Ar-H), 8.09-8.12 (d, 2H, *J* = 8.4 Hz, 2 × Ar-H), 11.02 (bs, 1H, NH) ppm. ^{13}C NMR (100 MHz, DMSO-d_6): δ 55.36, 111.78, 118.48, 122.06, 123.97, 125.54, 127.65, 128.13, 129.49, 130.50, 135.35, 138.90, 163.38, 163.62 ppm. ESI HRMS *m/z* calcd. for $C_{16}H_{11}ClN_6O$ $[M-(H)]^+$ 337.0605, found 337.0604. HPLC: t_R = 10.183 min (99% at 254 nm).

2-(5-(4-Chlorophenyl)-2H-tetrazol-2-yl)-N-(4-cyanophenyl)acetamide (**25**): Yield = 46%; white solid, mp = 228-230 °C; ^{1}H NMR (400 MHz, DMSO-d_6): δ 5.85 (s, 2H, CH_2), 7.66 (d, 2H, *J* = 8.6 Hz, 2 × Ar-H), 7.77 (d, 2H, *J* = 8.8 Hz, 2 × Ar-H), 7.83 (d, 2H, *J* = 8.8 Hz, 2 × Ar-H), 8.10 (d, 2H, *J* = 8.6 Hz, 2 × Ar-H), 11.10 (bs, 1H, NH) ppm. ^{13}C NMR (100 MHz, DMSO-d_6): δ 55.45, 105.87, 118.84, 119.43, 125.53, 128.13, 129.49, 133.49, 135.35, 142.28, 163.38, 163.78 ppm. ESI HRMS *m/z* calcd. for $C_{16}H_{11}ClN_6O$ $[M-(H)]^+$ 337.0605, found 337.0609. HPLC: t_R = 10.197 min (100% at 254 nm).

2-(5-(4-Chlorophenyl)-2H-tetrazol-2-yl)-N-phenylacetamide (**30**): Yield = 58%; white needles, mp = 210-212°C; ^{1}H NMR (400 MHz, DMSO-d_6): δ 5.79 (s, 2H, CH_2), 7.12 (t, 1H, *J* = 7.4 Hz, Ar-H), 7.35 (t, 2H, *J* = 7.9 Hz, 2 × Ar-H), 7.60 (d, 2H, *J* = 8.3 Hz, 2 × Ar-H), 7.66 (d, 2H, *J* = 8.5 Hz, 2 × Ar-H), 8.11 (d, 2H, *J* = 8.5 Hz, 2 × Ar-H), 10.66 (bs, 1H, NH) ppm. ^{13}C NMR (100 MHz, DMSO-d_6): δ 55.42, 119.30, 124.01, 125.60, 128.13, 128.96, 129.48, 135.31, 138.15 162.83, 163.33 ppm. ESI HRMS *m/z* calcd. for $C_{15}H_{12}ClN_5O$ $[M-(H)]^+$ 312.0652, found 312.0655. HPLC: t_R = 10.320 min (100% at 254 nm).

General procedure for synthesis of compounds **13** and **18**: To a cooled (0 °C) solution of nitrile (0.080 mg, 0.236 mmol) in DMSO, 30% H_2O_2 (0.5 mL) and 1 M NaOH were added (0.70 mL, 0.700 mmol). The reaction mixture was stirred for 4 h at room temperature. It was quenched with saturated aqueous Na_2SO_3. The formed precipitate was washed with water and recrystallized from ethanol to obtain pure final compounds.

3-(2-(5-(4-Chlorophenyl)-2H-tetrazol-2-yl)acetamido)benzamide (compound **13**): Yield = 59%; white solid, mp = 244-246 °C; ^{1}H NMR (400 MHz, DMSO-d_6): δ 5.87 (s, 2H, CH_2), 7.36 (bs, 1H, $CONH_{2a}$), 7.40 (t, 1H, *J* = 7.8 Hz, Ar-H), 7.59 (d, 1H, *J* = 8.8 Hz, Ar-H), 7.65 (d, 2H, *J* = 8.5 Hz, 2 × Ar-H), 7.82 (dd, 1H, J_1 = 7.8, J_2 = 1.9 Hz, Ar-H), 8.03 (bs, 1H, $CONH_{2b}$), 8.11 (d, 2H, *J* = 8.5 Hz, 2 × Ar-H), 8.19 (t, 1H, *J* = 1.9 Hz, Ar-H), 11.21(bs, 1H, NH) ppm. ^{13}C NMR (100 MHz, DMSO-d_6): δ 55.48, 119.06, 121.99, 122.68, 125.61, 128.14, 128.68, 129.47, 135.03, 135.28, 138.31, 163.09, 163.31, 167.58 ppm. ESI HRMS *m/z* calcd. for $C_{16}H_{13}ClN_6O_2$ $[M-(H)]^+$ 355.0737, found 355.0717. HPLC: t_R = 7.883 min (100% at 254 nm).

4-(2-(5-(4-Chlorophenyl)-2H-tetrazol-2-yl)acetamido)benzamide (compound **18**): Yield = 66%; white solid, mp = 252-255 °C; ^{1}H NMR (400 MHz, DMSO-d_6): δ 5.94 (s, 2H, CH_2), 7.28 (bs, 1H, $CONH_{2a}$), 7.66 (d, 2H, *J* = 8.6 Hz, 2 × Ar-H), 7.71 (d, 2H, *J* = 8.8 Hz, 2 × Ar-H), 7.86 (d, 2H, *J* = 8.8 Hz, 2 × Ar-H), 7.90 (bs, 1H, $CONH_{2b}$), 8.11 (d, 2H, *J* = 8.6 Hz, 2 × Ar-H), 11.31 (bs, 1H, NH) ppm. ^{13}C NMR (100 MHz, DMSO-d_6): δ 55.57, 118.56, 125.60, 128.13, 128.45, 129.39, 129.46, 135.28, 140.89, 163.32, 163.37, 167.26 ppm. ESI HRMS *m/z* calcd. for $C_{16}H_{13}ClN_6O_2$ $[M-(H)]^+$ 355.0710, found 355.0707. HPLC: t_R = 7.860 min (100% at 254 nm).

Identity and purity of screening hits:

2-(5-(4-Chlorophenyl)-2H-tetrazol-2-yl)-N-(4-methyl-3-nitrophenyl)acetamide (**26**): ^{1}H NMR (400 MHz, DMSO-d_6): δ 2.38 (s, 3H, CH_3), 5.85 (s, 2H, CH_2), 7.57 (s, 2H, 2 × Ar-H), 7.67 (d, 2H, *J* = 8.6 Hz, 2 × Ar-H), 7.83 (s, 1H, Ar-H), 8.10 (d, 2H, *J* = 8.6 Hz, 2 × Ar-H), 10.81 (bs, 1H, NH) ppm. ESI MS *m/z* calcd. for $C_{16}H_{13}ClN_6O_3$ $[M-(H)]^+$ 372.07, found 370.92, $[M+(Na)]^+$ 394.72. HPLC: HPLC: t_R = 11.514 min (92% at 254 nm).

Results and Discussion

Virtual Screening: Pharmacophore models are widely used as virtual screening filters and can be applied in ligand-based and structure-based design scenarios where compound databases are mapped to the pharmacophore model and key interactions are postulated for the hits of such VS studies.[33] With the help of recently available crystal structure information on MurB enzyme in complex with $NADP^+$ (PDB IDs: 4JAY, 4JB1) and available enzymatic data on MurB in complex with the substrate UDP-Glc*N*Ac-EP (PDB ID: 2MBR), the pharmacophore model was designed in a mixed ligand-based and structure-based manner. The pharmacophore model was used in a subsequent filtering step where previously curated ZINC-based LigandScout ldb conformer database was screened to identify an initial hit compound **13**. The details are described in Methods and Materials chapter.

Ligand-based drug design and biological evaluation: As the hit compound **13** showed promising inhibitory activity in low micromolar range (IC_{50} value of 34 µM), additional *in silico* analogue identification step was performed. From the compounds with highest similarity to **13**, available compounds **19**-**23** and **26**-**29** were obtained as presented in Table 2. Furthermore, we have decided to resynthesize VS screening hit **13** and to synthesize additional compounds **18**, **24**, **25** and **30** in order to analytically validate the studied structures and perform an initial structure-activity relationship study on the tetrazole compound set (Table 2). All additional 13 compounds were evaluated *in vitro* for their inhibition of *E. coli* MurB enzyme. The results are presented as residual activities (RAs) of MurB in the presence of 100 µM of each compound. For the compounds with RAs lower than 50%, the IC_{50} values were determined. It can be observed that *para*-chlorophenyl analogues display IC_{50} values from 25 to 90 µM with poorly tolerated chlorine atom replacements and relocations. The terminal *para*-carboxamide functional group is evidently not essential and can be replaced with nitrile or 4-methyl-3-nitro derivatized phenyl ring. This observation is in accordance with Gilbert *et al*. where structurally similar

series of pyrazolidine-3,5-dione inhibitors of MurB roughly occupied the same pocket above the FAD *N*-5 atom with the *para*-chlorophenyl moiety. [17]

The steady state analysis of enzyme kinetics was performed for the most potent compound **30**. The best model revealed non-competitive binding of inhibitor with respect to NADPH, with Ki value of 63 ± 10 µM. The models of inhibition with respect to UDP-Glc*N*Ac-EP showed no correlation. The positive control (compound **5**) was evaluated under the same conditions as our compounds and it inhibited MurB with an IC_{50} value of 20 ± 2 µM (literature value 11.4 µM). [18]

Molecular docking: Compounds **25**, **18**, **22**, **30**, **26** and **13** were the highest ranking and all shared similar predicted binding mode (Figure 8, c). The polar tetrazole core occupies the space of triphosphopyridine nucleotide sugar and phosphate, extending with the acetamido moiety towards the FAD *N*-5 atom, and Glu335 and Ser239 residues. Terminal *para*-chlorophenyl ring attached to the position 5 of the tetrazole core is favorable for inhibitory activity as relocation or substitution of chlorine atom led to inactive compounds. Similar observation was interestingly also reported by Gilbert *et al*. in the study of structurally similar series of pyrazolidine-3,5-dione inhibitors of MurB.[17] For reference, pyrazolidine-3,5-dione compound **7f** (Figure 8, c) reported by Kutterer *et al*., was also docked in our system where similar binding mode to tetrazole compounds was observed (Figure 8, c). Contrasting to *para*-chlorophenyl compounds, relocation of chlorine to *ortho*-position on phenyl ring or substitution of chlorine atom with *ortho*-methyl substituent resulted in a slightly altered binding mode according to our molecular docking study. It can be postulated that π-π stacking of *para*-chlorophenyl moiety between Tyr196 and Tyr264 residues is favorable with additional interactions between ligand tetrazol-acetamido central moiety towards Asn243 and Lys272 (Figure 8, b). Reported inhibitor **7f** by Kutterer *et al*. branches the scaffold with additional *para*-chlorophenyl moiety that extends towards Asn243, but our reported tetrazoles can favorably reach deeper in the main pocket towards FAD, where a carboxamde or similar functional group can interact with FAD. Compounds could be therefore described as structural continuation of 1,2-bis(4-chlorophenyl) pyrazolidine-3,5-diones reported beforehand.[16] We also compared the docked poses of our tetrazole compounds and aligned them to the starting pharmacophore model. We observed a good correlation between common binding mode of tetrazole compounds and essential structural features imposed by the starting pharmacophore model used in VS scenario (Figure 8, d).

Figure 8: a) Binding mode of compound **13** depicted in yellow; b) 2D projection of compound **13** in the active site with key interactions; c) Common binding mode observed for tetrazole compounds depicted yellow with superimposed docked pose of compound **7f** reported by Kutterer *et al*. (depicted in magenta); d) Aligned docked poses for reported tetrazole compound series to the developed pharmacophore model used in the first step for VS campaign.

Conclusion

In conclusion, a novel series of 5-substituted tetrazol-2-yl acetamido inhibitors of MurB have been identified through combined structure-based and ligand-based drug design methods. Several low micromolar inhibitors have been reported with compounds **13** (Figure 8, a), **26** and **30** displaying IC_{50} values of 34, 28 and 25 μM, respectively. If none of the tested compounds possessed *in vitro* antimicrobial activity against *S. aureus* and *E. coli*, the reported series nevertheless lends itself to further optimisation studies as similar scaffolds are reported in literature bearing antibacterial activity.[34] Furthermore, reported series is also of interest for biological evaluation of the compound effects on bacterial virulence. After a thorough analysis of the research field, this study is relevant in the context of antibacterial drug discovery, as there were few inhibitors reported up to date. Additional studies would enable further structure-activity relationship data, experimental insight into the binding modes and possible optimization towards antibacterial activity.

Abbreviations

FAD	flavin adenine dinucleotide
NADPH	β-nicotinamide dinucleotide phosphate
Mur*N*Ac	*N*-acetyl muramic acid
PEP	phosphoenolpyruvate
UDP	uridine 5'-diphosphate
UDP-Glc*N*Ac	UDP-*N*-acetyl glucosamine
UDP-GlcNAc-EP	UDP-N-acetyl glucosamine-enolpyruvate
HBD	H-bond donor pharmacophoric feature
HBA	H-bond acceptor pharmacophoric feature
VS	virtual screening

Conflict of interest

The authors declare they have no conflict of interest.

Acknowledgments

This study was supported by the Slovenian Research Agency (grants no. L1-6745, J1-6743 and Z1-8158). We thank Dr. Dušan Žigon (Mass Spectrometry Center, Jožef Stefan Institute, Ljubljana, Slovenia) for mass spectra. We also thank OpenEye Scientific Software (Santa Fe, New Mexico, USA) and Inte:Ligand (Software-Entwicklungs und Consulting GmbH, Maria Enzersdorf, Austria) for their help and support.

References

[1] E. D. Brown, G. D. Wright, *Nature* **2016**, *529*, 336.

[2] K. Bush, *Future Med. Chem.* **2016**, *8*, 921.

[3] K. Lewis, *Nat. Rev. Drug Discov.* **2013**, *12*, 371.

[4] M. Hrast, I. Sosič, R. Šink, S. Gobec, *Bioorg. Chem.* **2014**, *55*, 2.

[5] H. Gelband *et al*., CDDEP Report. The State of the World's Antibiotics, **2015**, http://cddep.org/publications/state_worlds_antibiotics_2015

[6] T. D. H. Bugg, D. Braddick, C. G. Dowson, D. I. Roper, *Trends Biotechnol.* **2011**, *29*, 167.

[7] W. Vollmer, D. Blanot, M. A. De Pedro, *FEMS Microbiol. Rev*. **2008**, *32*, 149.

[8] H. Barreteau, A. Kovač, A. Boniface, M. Sova, S. Gobec, D. Blanot, *FEMS Microbiol. Rev*. **2008**, *32*, 168.

[9] T. Schneider, H-G. Sahl, *Int. J. Med. Microbiol.* **2010**, *300*, 161.

[10] D. W. Green, *Expert Opin. Ther. Targets* **2002**, *6*, 1.

[11] T. E. Benson, C. T. Walsh, J. M. Hogle, *Structure* **1996,** *4*, 47.

[12] M. W. Chen, B. Lohkamp, R. Schnell, J. Lescar, G. Schneider, *PLoS ONE*, **2013**, *8*, 1.

[13] C. J. Andres, J. J. Bronson, S. V. D'Andrea, M. S. Deshpande, P. J. Falk, K. A. Grant-Young, W. E. Harte, H-T. Ho, P. F. Misco, J. G. Robertson, D. Stock, Y. Sun, A. W. Walsh. *Bioorg. Med. Chem. Lett*. **2000**, *10*, 715.

[14] J. J. Bronson, K. L. DenBleyker, P. J. Falk, R. A. Mate, H-T. Ho, M. J. Pucci, L. B. Snyder. *Bioorg. Med. Chem. Lett*. **2003**, *13*, 873.

[15] R. W. Sarver, J. M. Rogers, D. E. Epps, *J. Biomol. Screen*. **2002,** *7*, 21.

[16] K. M. K. Kutterer, J. M. Davis, G. Singh. Y. Yang, W. Hu, A. Severin, B. A. Rasmussen, G. Krishnamurthy, A. Failli, A. H. Katz, *Bioorg. Med. Chem. Lett*. **2005**, *15*, 2527.

[17] A. M. Gilbert, A. Failli, J. Shumsky, Y. Yang, A. Severin, G. Singh, A. H. Katz*, J. Med. Chem*. **2006**, *49*, 6027.

[18] G. D. Francisco, Z. Li, J. D. Albright, N. H. Eudy, A. H. Katz, P. J. Petersen, P. Labthavikul, G. Singh, Y. Yang, B. A. Rasmussen, Y. I. Lin, T. S. Mansour, *Bioorg. Med. Chem. Lett*. **2004**, *14*, 235.

[19] J. J. Irwin, B. K. Shoichet, *J. Chem. Inf. Model*. **2005**, *45*, 177.

[20] C. G. Wermuth, C. R. Ganellin, P. Lindberg, L. A. Mitscher, *Pure Appl. Chem*. **1998**, *70*, 1129.

[21] G. Wolber, T. Langer, *J. Chem. Inf. Model*. **2005**, *45*, 160.

[22] T. E. Benson, C. T. Walsh, J. M. Hogle, *Biochemistry* **1997**, *36*, 806.

[23] G. Wolber, A. A. Dornhofer, T. Langer, *J. Comput. Aided Mol. Des.* **2006**, *20*, 773.

[24] S. L. McGovern, B. T. Helfand, B. Feng, B. K. Shoichet, *J. Med. Chem.* **2003**, *46*, 4265.

[25] J. B. Baell, G. A. Holloway, *J. Med. Chem.* **2010**, *53*, 2719.

[26] W. P. Walters, M. Namchuk, *Nat. Rev. Drug Discov.* **2003**, *2(4),* 259.

[27] P. C. D. Hawkins, A. G. Skillman, G. L. Warren, B. A. Ellingson, M. T. Stahl, *J. Chem. Inf. Model.* **2010**, *50*, 572.

[28] K. E., Hevener, W. Zhao, D. M. Ball, K. Babaoglu, J. Qi, S. W. White, R. E. Lee (2009). *J. Chem. Inf. Model.* **2009**, 49(2), 444-460.

[29] N. M. O'Boyle, M. Banck, C. A. James, C. Morley, T. Vandermeersch, G. R. Hutchison, *J. Cheminform*. **2011**, *3(1),* 33.

[30] T. E. Benson, J. L. Marquardt, A. C. Marquardt, F. A. Etzkorn, C. T. Walsh, *Biochemistry* **1993**, *32*, 2024.

[31] European Committee for Antimicrobial Susceptibility Testing of the European Society of Clinical M, Infectious D. Determination of minimum inhibitory concentrations (MICs) of antibacterial agents by broth dilution. *Clin. Microbiol. Infect.* **2003**, *9(8),* IX.

[32] A. K. Valiveti, U. M., Bhalerao, J. Acharya, H. N. Karade, R. Gundapu, A. K. Halve, M. P. Kushik, *Chem. Biol. Interact.* **2015**, *237*, 125.

[33] Q. Gao, L. Yang, Y. Zhu, *Curr. Comput. Aided Drug Des.* **2010**, *6*, 37.

[34] B. Manjunatha, G. K. Nagaraja, K. Reshma, S. K. Peethamber, M. R. Shafeeulla, *RSC Adv*., **2016**, 6, 59375–59388.

Figure Legends and Tables

Figure 1: Catalytic consecutive and two-step mechanism of MurB.

Figure 2: Previously described MurB inhibitors present in the scientific literature.

Figure 3: Left: pharmacophore, created on the basis of NADP, chain A (PDB ID: 4JAY) with superposed shared pharmacophore with UDP-GlcNAc-EP (PDB ID: 2MBR). Middle: pharmacophore, created with superposed NADP. Right: pharmacophore, created with added exclusion sphere coat representing the available space in the active site (yellow – planar/aromatic with tolerance sphere of 1.5 Å, red – H-bond acceptor with vector and tolerance sphere of 1.5 Å, green – H-bond donor with vector and tolerance sphere of 1.5 Å, centered red sphere – ionisable feature with tolerance of 2.15 Å, grey – exclusion spheres with tolerance of 1 Å).

Figure 4: Left: superposition of UDP-GlcNAc-EP (blue, PDB ID: 2MBR) and NADP (cyan with coloured atom types, PDB ID: 4JAY); FAD can be observed in almost identical binding mode. Right: calculated pharmacophore: hydrophobic 46.571907, -5.837457, 11.458156; ionisable 45.4222 -11.2288 11.2484; ionisable 45.8758 -13.7696 11.946; HBA 52.896 -10.663 12.334, 50.177 -10.402 13.677; HBA 53.257 -9.782 15.791, 50.177 -10.402 13.677; HBA 47.614 -13.199 7.989, 47.208 -13.871 11.119; HBA 43.817, -13.738, 7.969, 45.229 -11.925 9.78; HBA 47.614 -13.199 7.989, 45.229 -11.925 9.78; HBA 43.132 -3.175 13.229, 45.933 -2.903 13.325; HBD 47.234 -3.916 14.773; 46.564 -1.598 16.459.

Figure 5: Preparation of ZINC database for virtual screening.

Figure 6: Lineweaver-Burk diagram of non-competitive binding mode of compound **30** versus NADPH. The concentration of NADPH (25, 50, 75, 100 and 200 μM) was varied at fixed concentration of UDP-Glc*N*Ac-EP (50 μM). The concentrations of inhibitor were 0, 10, 20, 30, 50, 75 and 100 μM.

Figure 7: Synthesis of tetrazoles. Reagents and conditions: (a) NaN_3, NH_4Cl, DMF, 120 °C, 18 h; (b) chloroacetyl chloride, TEA, DCM, 0°C - rt, 6 h; (c) KOH, EtOH, reflux, 16 h; (d) 30% H_2O_2, 1 M NaOH, DMSO, 0°C - rt, 4 h.

Figure 8: a) Binding mode of compound **13** depicted in yellow; b) 2D projection of compound **13** in the active site with key interactions; c) Common binding mode observed for tetrazole compounds depicted yellow with superimposed docked pose of compound **7f** reported by Kutterer *et al*. (depicted in magenta); d) Aligned docked poses for reported tetrazole compound series to the developed pharmacophore model used in the first step for VS campaign.

Table 1: Top scoring and commercially available compounds after VS and biological evaluation.

No	*Structure*	*VS score*[a]	*RA (%)*[b]	*No*	*Structure*	*VS score*[a]	*RA (%)*[b]
6	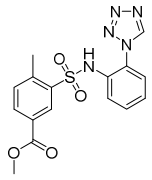	95.37	100	**12**	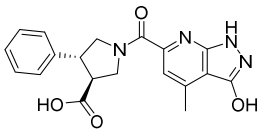	95.25	71
7	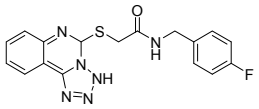	95.34	/	**13**	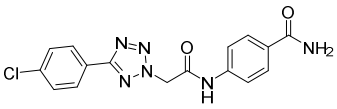	95.32	**22 IC_{50} = 34 ± 4 µM**
8	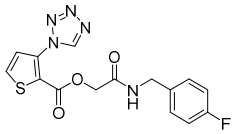	95.31	100	**14**	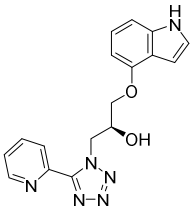	95.42	97
9	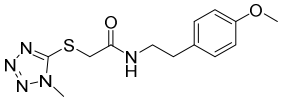	95.67	100	**15**	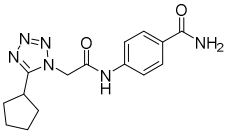	95.34	71
10	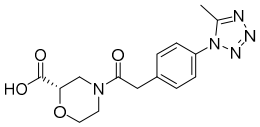	75.41	100	**16**	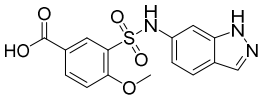	94.33	100
11	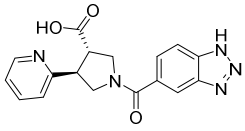	95.59	83	**17**	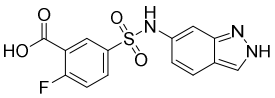	94.70	78

[a] Pharmacophore [b] Residual activity (in %) of the enzyme at 100 µM tested compound.

Table 2: Structural analogues of the hit compound **13** and their biological evaluation on MurB enzyme.

No	*Structure*	*RA (%)[b] or IC50 (μM)[c]*	*No*	*Structure*	*RA (%)[b] or IC50 (μM)[c]*
13	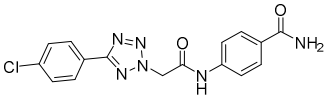	34 ± 3 μM	**24**	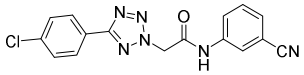	51 ± 5 μM
18	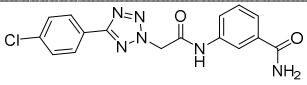	90 ± 8 μM	**25**	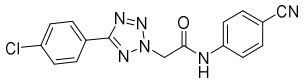	76%
19	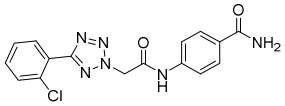	75%	**26**	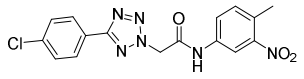	28 ± 3 μM
20	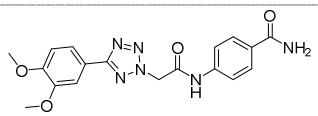	84%	**27**	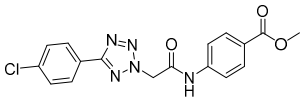	79%
21	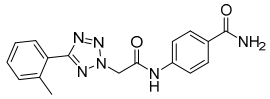	98%	**28**	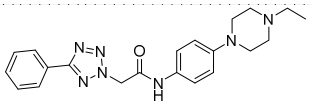	82%
22	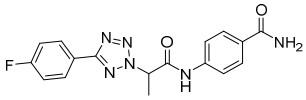	71%	**29**	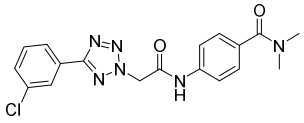	70%
23	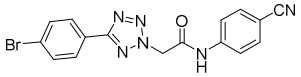	62%	**30**	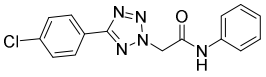	25 ± 2 μM

[b] Residual activity (%) of the enzyme at 100 μM tested compound. [c] IC_{50} (μM) determined from 7 concentrations and curve fitted with logit-log plot.

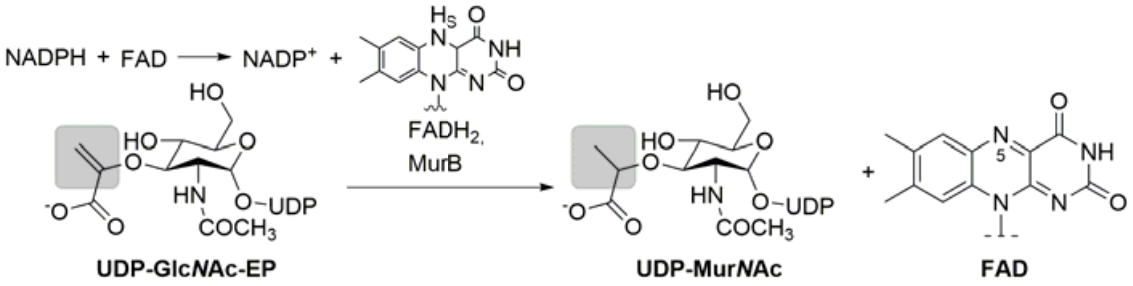

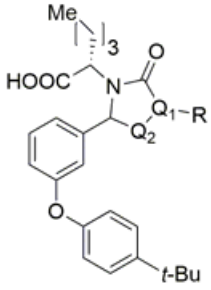

1

Q_1=C(sp^3); Q_2=S; R=H

2

Q_1=N; Q_2=C(sp^2); R=Bn

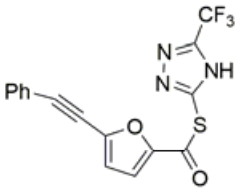

3

K_d (*S. aureus*) = 0.14 μM

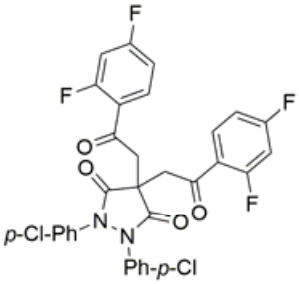

4

Ph-*p*-Cl - *para*-chlorophenyl

IC_{50} (*E. coli*) = 5.8 μM

MIC (MRSA) = 12.5 μM

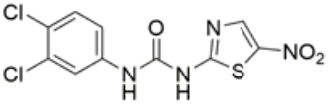

5

IC_{50} (*E. coli*) = 3.8 μM